Systems & Control Transactions

Original Research Article
Peer Reviewed Conference Proceeding
ESCAPE 36 - European Symposium on Computer Aided Process Engineering
Sheffield, UK. 21-24 June 2026

PSE PRESS

CFD-based optimal design of a portable and stackable alkaline water electrolyser for hydrogen production

Akepogu Venkateshwarlu[a], Gianluca Li-Puma[ab], and Brahim Benyahia[a]*

[a] Department of Chemical Engineering, Loughborough University, LE11 3TU Leicestershire, UK
[b] Chemical and Environmental Engineering, University of Palermo, Piazza Marina, 61 90133 Palermo, Italy
* Corresponding Author: b.benyahia@lboro.ac.uk.

ABSTRACT

Hydrogen is increasingly recognized as a vital energy carrier for a sustainable future. Among the various methods for hydrogen production, alkaline water electrolysis (AWE) stands out as a well-established and commercially viable option. However, their more effective deployment requires more advanced, portable, and scalable designs. This study explores systematic model-based shape optimization of the next generation AWE based on computational fluid dynamic (CFD) aimed to enhance the hydrodynamics and electrochemical performance. Several design geometries and arrangements were proposed including flow baffles to enhance hydrodynamic and facilitate detachment of oxygen and hydrogen bubbles. The findings indicate that the optimal design and location of the baffles improve fluid mixing and enhance bubble detachment, resulting in a more uniform electrolyte distribution and decreased concentration polarization. Several key performance indicators were considered to analyse the performance of proposed designs including gas production rates, polarization curves, and fluid flow velocity profiles. The insights gained from this research offer valuable recommendations for optimizing flow field designs in alkaline water electrolyzers, aiming to enhance efficiency and operational robustness.

Keywords: Alkaline water electrolysis, zero-gap cell, CFD, Pyramidal pins, Mesh electrode, Multiphysics model

INTRODUCTION

Hydrogen is becoming essential in the transition to decarbonized energy systems, influenced by climate targets and energy security [1, 2]. The global demand for hydrogen is expected to increase significantly, shifting from fossil-based “grey hydrogen” to low-carbon “green hydrogen, ” produced through water electrolysis using renewable energy [3]. Hydrogen production via water electrolysis is a key enabling technology for future low-carbon energy systems[4]. There are three primary methods for water electrolysis: alkaline water electrolysis (AWE), proton exchange membrane electrolysis (PEM), and solid oxide electrolysis (SOEC) and among them, alkaline water electrolysis (AWE) is the most established for hydrogen production [1, 3–6]. It offers advantages such as lower material costs, reliance on non-noble catalysts, longer stack lifetimes, and scalability for large deployments, especially in regions abundant in renewable resources [5, 7, 8]. AWE's reliability and adaptability to variable operating conditions are crucial as electrolysis facilities align with fluctuating renewable energy supplies. This adaptability makes AWE an economically viable option for large-scale hydrogen production [9, 10]. As the world moves towards sustainable energy solutions, AWE is positioned to play a significant role in meeting the rising demand for green hydrogen[4].

Alkaline water electrolysis (AWE) faces significant challenges due to complex hydrodynamics, particularly the behavior of gas bubbles at the electrode-electrolyte interface [6, 11, 12]. These bubbles can create localized concentration gradients, increase ohmic losses, and generate thermal hotspots, ultimately diminishing energy efficiency [12]. Factors such as electrode shape, channel geometry, operating conditions, and cell integration strategies influence the distribution of gas and liquid, making the optimization of bubble behavior and internal flow essential for enhancing system performance [7, 9, 11]. Traditional AWE designs often utilize concave-convex spherical (SCC) flow channels to improve mixing; however, these can also lead to stagnant regions and bubble trapping, resulting in non-uniform mass transfer

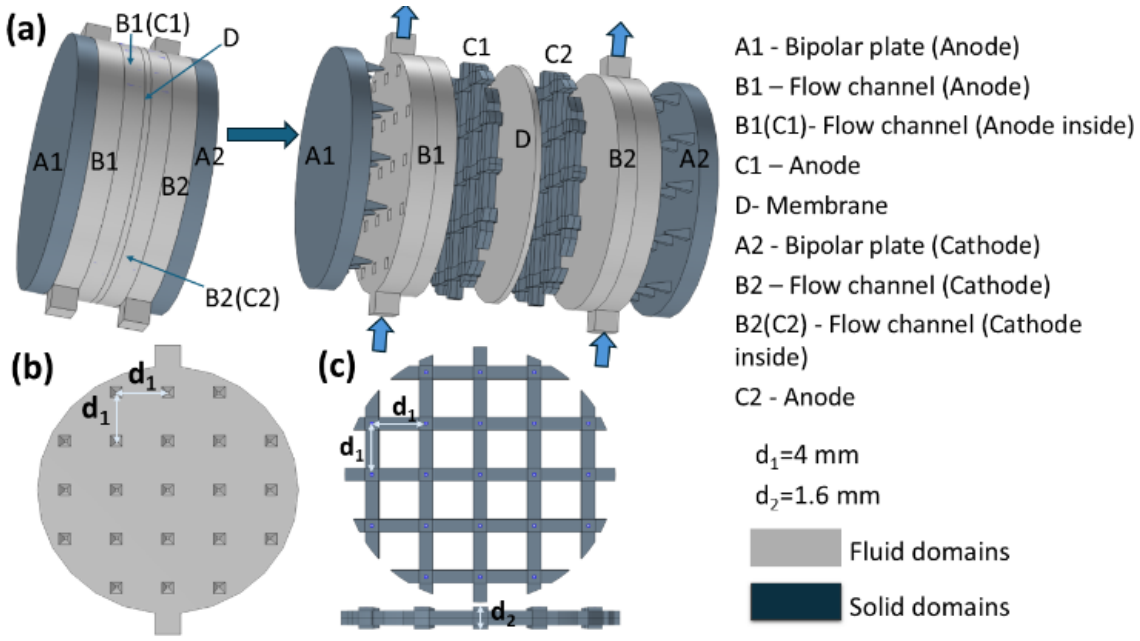

Figure 1. Schematics of the alkaline wate electrolyser with individual components, (b) arrangment of the pyramidal pins in the flow channel, and (c) mesh electrode.

[12]. A potential solution involves replacing porous electrodes with mesh-type structures, which may decrease bubble residence time and improve gas release [13]. Nonetheless, the interplay between mesh electrodes, SCC flow fields, and various operational variables have yet to be thoroughly investigated in a cohesive framework.

With increasing computational power, computational fluid dynamics (CFD) methods have gained widespread adoption across multiple disciplines. These methods have been widely implemented to support the optimal design and operation of multiphase systems across multiple scales, from microfluidic devices to mesoscale processes and full industrial-scale systems [14, 15]. Recent CFD applications highlight systematic geometry and shape optimization of small-scale packed-bed reactors with complex internal structures [16]. These methods have opened new opportunities for more effective in silico prototyping, enabling faster design, evaluation, and optimization of next-generation processes and technologies. The proposed CFD-based design framework of zero-gap alkaline electrolyzers allows more robust geometries and configuration through a detailed three-dimensional multiphysics simulation which addresses the limitations of the existing designs. The method incorporates crucial aspects such as heat transfer, gas-liquid transport, and electrochemical kinetics, facilitating a comprehensive assessment of how localized gradients affect system performance. The model evaluates critical parameters including cell voltage, temperature, and inlet flowrate collectively, revealing their interactions and providing insights for optimizing device performance beyond single-parameter analysis. Most importantly, the CFD-based approach reveals more effective alternatives to the traditional porous electrodes such as mesh-type electrodes, enhancing productivity and hydrodynamic performance particularly more effective bubble detachment and transport. The identified optimal designs featuring pyramidal pin structures on the bipolar plates. The method also informed the best trade-offs between mixing and bubble detachment. Ultimately the framework offers essential design insights laying the foundation for enhanced efficiency and durability of industrial green hydrogen production systems.

METHODOLOGY

A numerical model representing a single cell of an alkaline water electrolyzer is illustrated in **Figure 1**. The computational domain encompasses flow channels, cathode and anode mesh electrodes, bipolar plates, and a porous membrane region that separates the two half-cells. The electrodes are of non-porous made of Nickel metal. Pyramidal pin structures are integrated into the flow channels and attached to the bipolar plates, with sharp edges oriented towards the electrodes to enhance flow distribution and induce local turbulence. The geometric dimensions and physical properties are detailed in **Table 1** and **Table 2**.

Table 1: Geometric parameters of the alkaline water electrolyser model.

Description	Value
Cathode and anode radius	10 mm
Cathode thickness	1.6 mm
Anode thickness	1.6 mm
Flow channel radius	10.1 mm
Flow channel thickness	3.6 mm
Bipolar plate radius	10 mm
Bipolar plate thickness	0.5 mm
Membrane radius	10.1 mm
Membrane thickness	0.5 mm

Table 2: Physical parameters of the alkaline water electrolyser model.

Parameter	Value
Membrane porosity	0.5
Reference exchange current density (anode)	100 A/m^2
Reference exchange current density (cathode)	0.1
Transfer coefficient (anode)	0.5
Transfer coefficient (anode)	0.5
Inlet electrolyte velocity	0.01 m/s - 0.2 m/s
Outlet pressure	1 atm
Electrolyte conductivity	40 S/m
Bipolar plate conductivity	4.032e6 S/m
Nickel mesh electrode conductivity	13.8e6 S/m
Electrode active surface area	6.06 cm^2
Operating temperature	80 C
Cell voltage	1.3 V – 2.3 V
Electrolyte concentration (KOH)	3 M

Governing equations

The following equations are employed to solve the physics described above:

Electrochemical model

Alkaline water electrolysis splits water into hydrogen and oxygen using electrochemical reactions at the cathode and anode. An aqueous alkaline solution like KOH serves as the electrolyte, supplying hydroxide ions (OH^-) for charge transport, driven by electrical potential.

At cathode (hydrogen evolution reaction – HER):

$$2H_2O + 2e^- \rightarrow H_2 + 2OH^- \quad (1)$$

At anode (oxygen evolution reaction – OER):

$$4OH^- \rightarrow O_2 + 2H_2O + 4e^- \quad (2)$$

The total cell voltage is calculated by

$$E_{total} = E_{equi} + \eta_{acti} + \eta_{ohmic} \quad (3)$$

The equilibrium cell potential is calculated from the Nernst equation as follows:

$$E_{equi} = E_{0,ref}(T) + \frac{RT}{2F}\ln\left(\frac{p(O_2)^{0.5}p(H_2)}{p(H_2O)}\right) \quad (4)$$

The Butler-Volmer equation describes the relationship between the local current density and activation overpotential as follows:

$$i_{cathode} = a_{HER}i_{0,HER}(1 - s_g)\left[exp\left(\frac{\alpha_c F\eta_{HER}}{RT}\right) - exp\left(\frac{(1-\alpha_c)F\eta_{HER}}{RT}\right)\right] \quad (5)$$

$$i_{anoode} = a_{OER}i_{0,OER}(1 - s_g)\left[exp\left(\frac{\alpha_a F\eta_{OER}}{RT}\right) - exp\left(\frac{(1-\alpha_a)F\eta_{OER}}{RT}\right)\right] \quad (6)$$

The equations for the transport of electrons and ions are given below:

$$\nabla \cdot \boldsymbol{i}_s = \nabla \cdot \left(-\sigma_s^{eff}\nabla\phi_s\right) = S_{\phi,s} \quad (7)$$

$$\nabla \cdot \boldsymbol{i}_l = \nabla \cdot \left(-\sigma_l^{eff}\nabla\phi_l\right) = S_{\phi,l} \quad (8)$$

$$\sigma_l^{eff} = \sigma_l(1 - s_g)^{1.5} \quad (9)$$

The ohmic overpotential resulting from the transport resistances of both electrons and ions is described as follows:

$$\eta_{ohmic} = i\left(\frac{\phi_l}{\sigma_l^{eff}} + \frac{\phi_s}{\sigma_s^{eff}}\right) \quad (10)$$

Mass transfer model

The Navier-Stokes equations are employed to determine the fluid velocity and pressure within the flow channels of the electrolyzer in the following manner.:

$$\frac{\partial\rho}{\partial t} + \nabla \cdot (\rho\boldsymbol{u}) = 0 \quad (11)$$

$$\rho\frac{\partial\boldsymbol{u}}{\partial t} + \rho(\boldsymbol{u} \cdot \nabla)\boldsymbol{u} = \nabla \cdot \left[-p\boldsymbol{I} + \mu\left(\nabla\boldsymbol{u} + (\nabla\boldsymbol{u})^T\right)\right] + \boldsymbol{F} \quad (12)$$

The phase transport equations have been adopted to describe the distribution of gas-liquid flow as follows:

$$\frac{\partial\rho_i s_i}{\partial t} + \nabla \cdot (\rho_i\boldsymbol{u}_i) = 0 \quad (13)$$

$$\frac{\partial\rho_i s_i}{\partial t} + \nabla \cdot \left[-\rho_i K\frac{K_{ri}}{\mu_i}(\nabla p_i - \rho_i\boldsymbol{g})\right] = Q_i \quad (14)$$

$$Q_{H_2} = \frac{M_{H_2}}{2F}i_v \quad (15)$$

$$Q_{O_2} = \frac{M_{O_2}}{4F}i_v \quad (16)$$

Heat transfer model

The energy equation has been employed to describe the thermal management inside the electrolyser:

$$(\rho C_p)_{eff}\frac{\partial T}{\partial t} + \rho C_p\boldsymbol{u} \cdot \nabla T + \left(-k_{eff}\nabla T\right) = S_{heat} \quad (17)$$

$$S_{heat} = |i_v||\eta_{acti}| + \frac{i_v^2}{\sigma_s} + \frac{i_v^2}{\sigma_l} \quad (18)$$

The governing equations delineated herein were resolved utilizing CFD through the COMSOL Multiphysics 6.4, employing the finite element method (FEM) [12]. A convergence criterion of relative error less than 0.0001 is applied, using the backward difference formula (BDF) method for time-stepping. This analysis was conducted under specific boundary conditions and underlying assumptions.

Boundary conditions

The KOH electrolyte solution enters the flow channels of anode and cathode at their inlets with a defined velocity, respectively. The cell voltage is applied on the bipolar plate and other side of the bipolar is made electric ground. The pressure at the outlets of the flow channels is 0 atm. The gravitational forces during the operation are neglected. The OH^- ions are allowed to pass through the porous membrane.

Assumptions

The flow is assumed to be laminar. There is no crossover of hydrogen and oxygen gases across the membrane. Overpotential losses due to contact resistance inside the electrolyser are assumed to be negligible.

RESULTS AND DISCUSSION

Validation

To assess the accuracy of the multi-physics alkaline electrolyzer model, operational parameters from existing literature were employed [12, 17], specifically at 353.15 K and 1 atm, as shown in **Figure 2**. A comparative evaluation of simulation outcomes alongside experimental data [17] and other literature simulations [12] shows a strong correlation within a current density range of 0.1 $\mathrm{A/cm^2}$ to 1.4 $\mathrm{A/cm^2}$. However, at higher current densities, simulated voltages exhibit slight underestimations, likely attributable to the omission of ohmic losses and diffusion voltage effects.

Effect of pyramidal pins on the velocity distribution

The study analyzed the effect of inlet electrolyte velocity on flow patterns in channels with 10 and 24 pyramidal pins on each side of the electrode, as shown in **Figures 3** and **4**. It has been observed that the flow patterns at velocities from 0.01 m/s to 0.2 m/s demonstrated that the pyramidal pin structures induced changes in the flow field, including local redirection, shear-layer formation, and wake recirculation. These alterations were found to depend significantly on both the inlet velocity and the number of the pins.

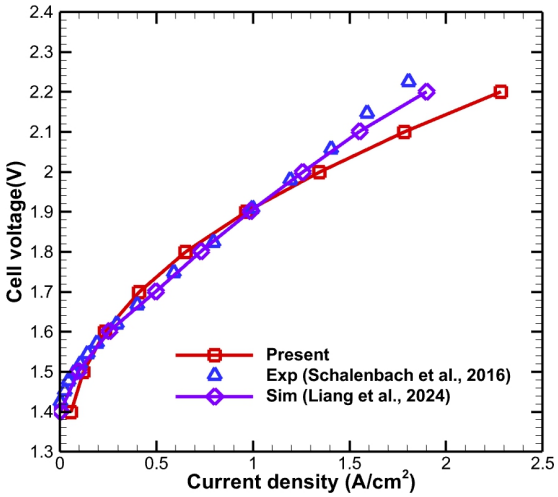

Figure 2. Comparison of the present simulation results against the experimental data [17] and other literature simulations [12].

At low velocity of 0.01 m/s, electrolyte motion was dominated by viscous forces. The 10 pins configuration caused minimal axial flow disruption (refer to **Figure 4(a)**), while the 24 pins setup resulted in increased tortuosity and narrower passages (refer to **Figure 4(a)**), leading to longer residence times and persistent recirculation zones, highlighting significant micro-circulation effects typically seen in creeping flow. Increasing inlet velocities of 0.05 m/s and 0.1 m/s intensified inertial effects, enhancing flow separation and wake formation. Higher pyramidal pin number improved hydrodynamic interactions, promoting vortex-dominated flow, which is crucial for enhancing bubble detachment and gas-liquid mass transfer in electrolyzer channels (refer to **Figures 3(b)-(c)** and **4(b)-4(c)**). At 0.2 m/s, strong convection dominated the flow field. In a 10 pins setup, limited recirculation occurred, while a 24 pins configuration enhanced flow complexity and inter-sphere mixing, resulting in maximum velocity uniformity and minimized small eddies with larger wake structures (refer to **Figures 3(d)** and **4(d)**).

Effect of inlet velocity on the gas volume fraction

The two-phase behavior in the channel arises from the hydrogen evolution reaction at the nickel mesh cathode in alkaline conditions. Gas bubbles form, grow, and detach due to nickel's wettability, leading to localized gas accumulation and high hydrogen volume near the cathode. Inlet electrolyte velocity impacts gas volume fraction distribution, as depicted in **Figures 5** and **6**. At 0.01 m/s, insufficient shear fails to remove bubbles from nickel mesh, increasing residence time and coalescence, leading to higher gas fractions near the cathode, reducing active surface area and hindering reactant replenishment

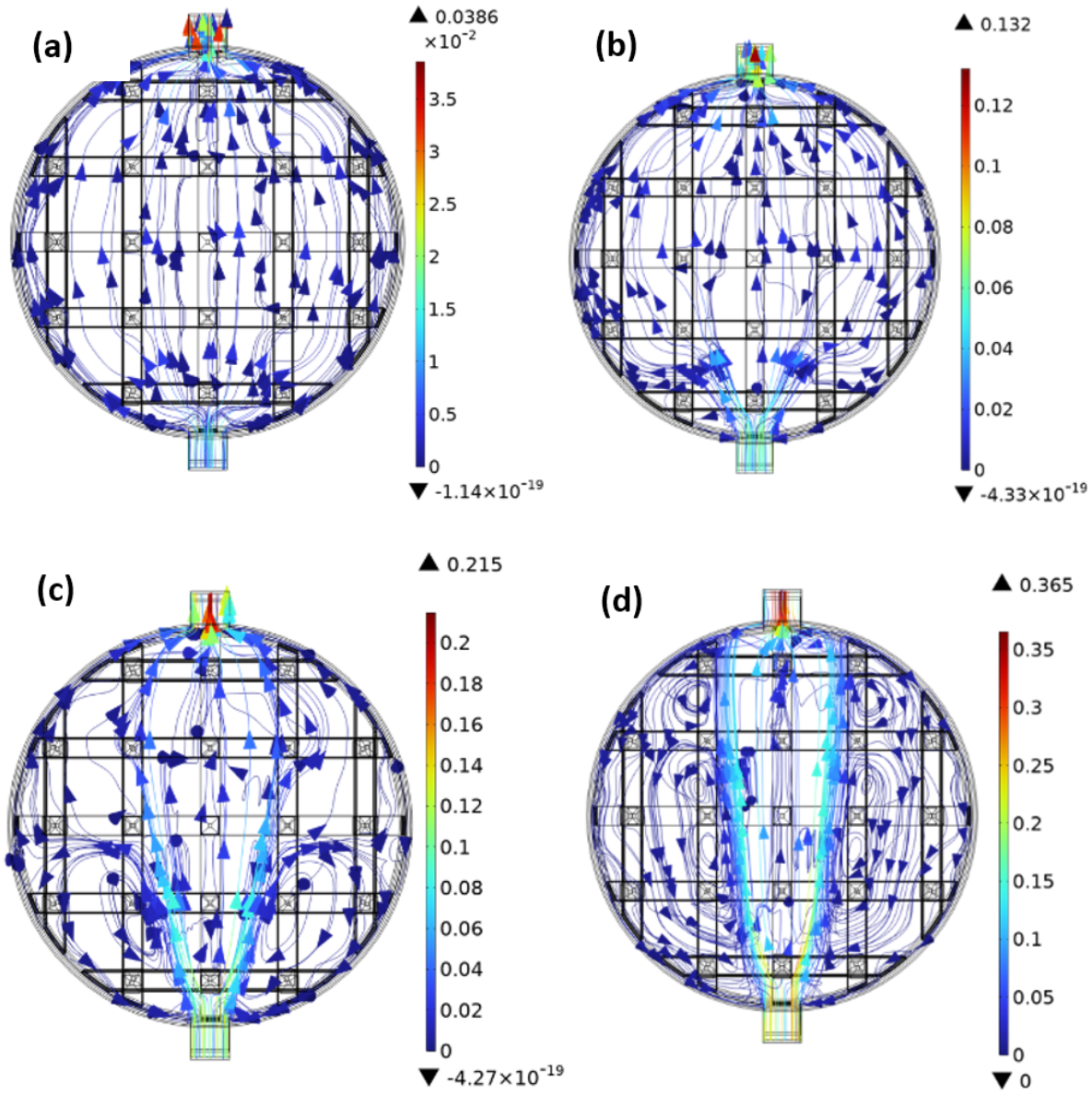

Figure 3. Velocity distribution in channels for 24 pyramidal pins, (a) $v_{in} = 0.01\ m/s$, (b) $v_{in} = 0.05\ m/s$, (c) (a) $v_{in} = 0.1\ m/s$, and (a) $v_{in} = 0.2\ m/s$.

(refer to **Figures 5(a)** and **6(a)**). Increasing inlet velocity to 0.05–0.1 m/s improved hydrogen bubble removal by enhancing convective forces, reducing gas volume fraction near the cathode. This facilitated electrolyte access to nickel sites, minimized gas holdup, and maintained efficient gas-evolving cathode performance without raising channel pressure losses (refer to **Figu res 5(b)-(c)** and **6(b)-4(c)**). At 0.2 m/s, the gas volume fraction was minimized, with rapid bubble detachment reducing interaction time with the nickel surface (refer to **Figures 5(d)** and **6(d)**). This inhibited coalescence, promoting effective mass transfer and bubble removal, though it may require higher pumping power for the system.

The study demonstrated minimal differences in gas volume fraction distributions within channels featuring 10 versus 24 pyramidal pins at varying velocities. While heightened pins number improved fluid tortuosity and localized micro-mixing, it did not significantly influence hydrogen bubble retention or removal on nickel mesh, underscoring the inlet velocity's critical impact on hydrogen gas holdup dynamics.

CONCLUSIONS

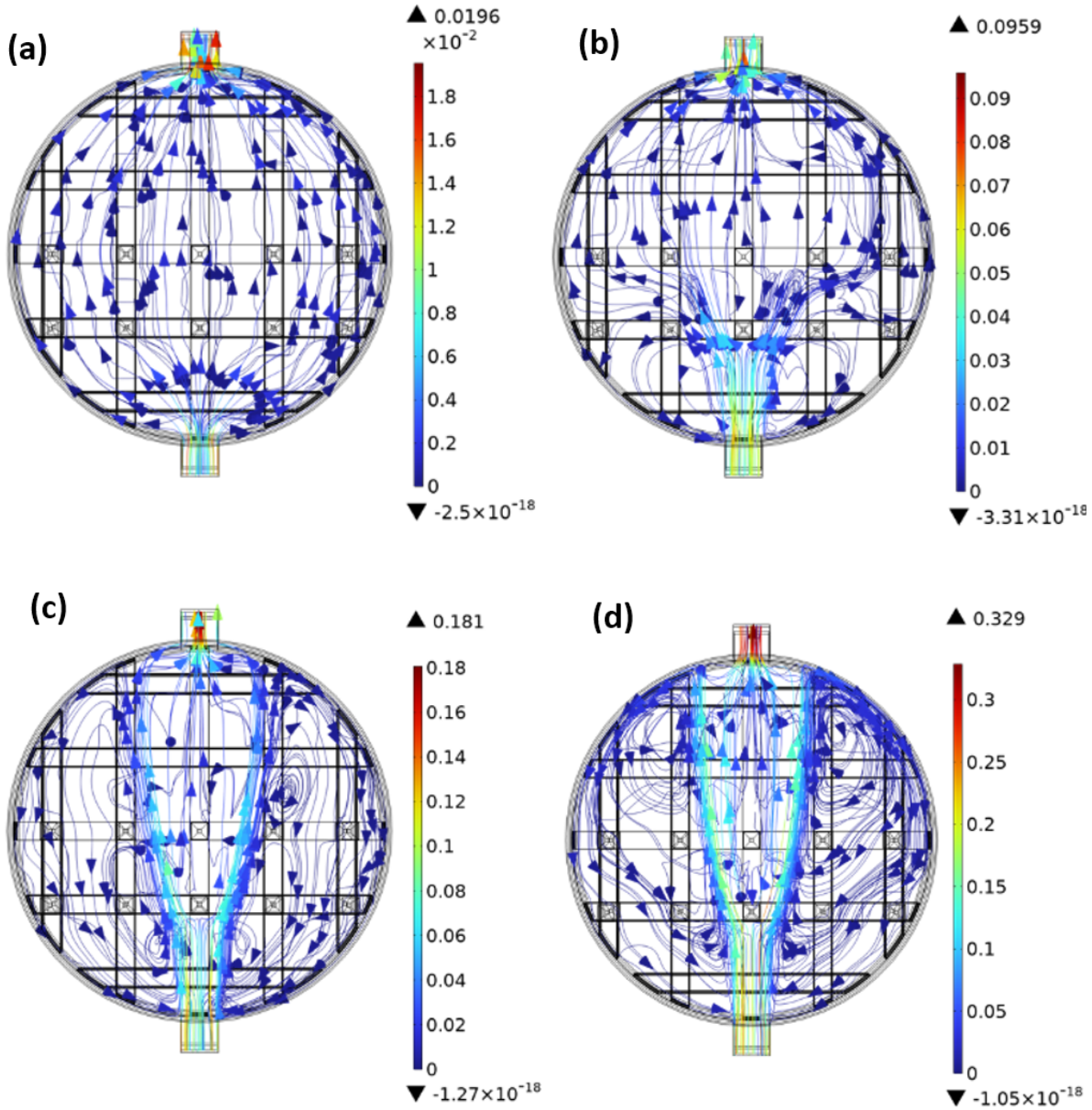

Figure 4. Velocity distribution in channels for 10 pyramidal pins, (a) $v_{in} = 0.01\ m/s$, (b) $v_{in} = 0.05\ m/s$, (c) (a) $v_{in} = 0.1\ m/s$, and (a) $v_{in} = 0.2\ m/s$.

A three-dimensional multiphysics model was developed to optimal design of a portable and stackable AWE for hydrogen production exhibiting two-phase flow dynamics and featuring nickel mesh electrodes, augmented by pyramidal pins to enhance flow disturbance and mixing. The simulations, conducted in COMSOL at a voltage of 1.8 V, 3 M KOH and a temperature of 80°C, were rigorously validated for reliability and accuracy. The findings indicated that the inlet elect rolyte velocity plays a pivotal role in hydrogen bubble detachment and gas holdup; specifically, lower velocities resulted in increased gas fractions due to bubble retention, whereas higher velocities facilitated bubble removal. Although increasing the number of pins improved flow tortuosity and micromixing, it did not significantly influence bubble detachment, suggesting that bubble dynamics are predominantly governed by bubble growth kinetics and convective shear forces. These findings imply that enhancing convective flow in proximity to gas-evolving electrodes can mitigate mass transfer limitations and enhance electrolyzer efficiency. Future research should prioritize the optimization of pyramidal pin design to maximize mixing while minimizing pressure drop challenges, advocating for multi-objective optimization to inform the

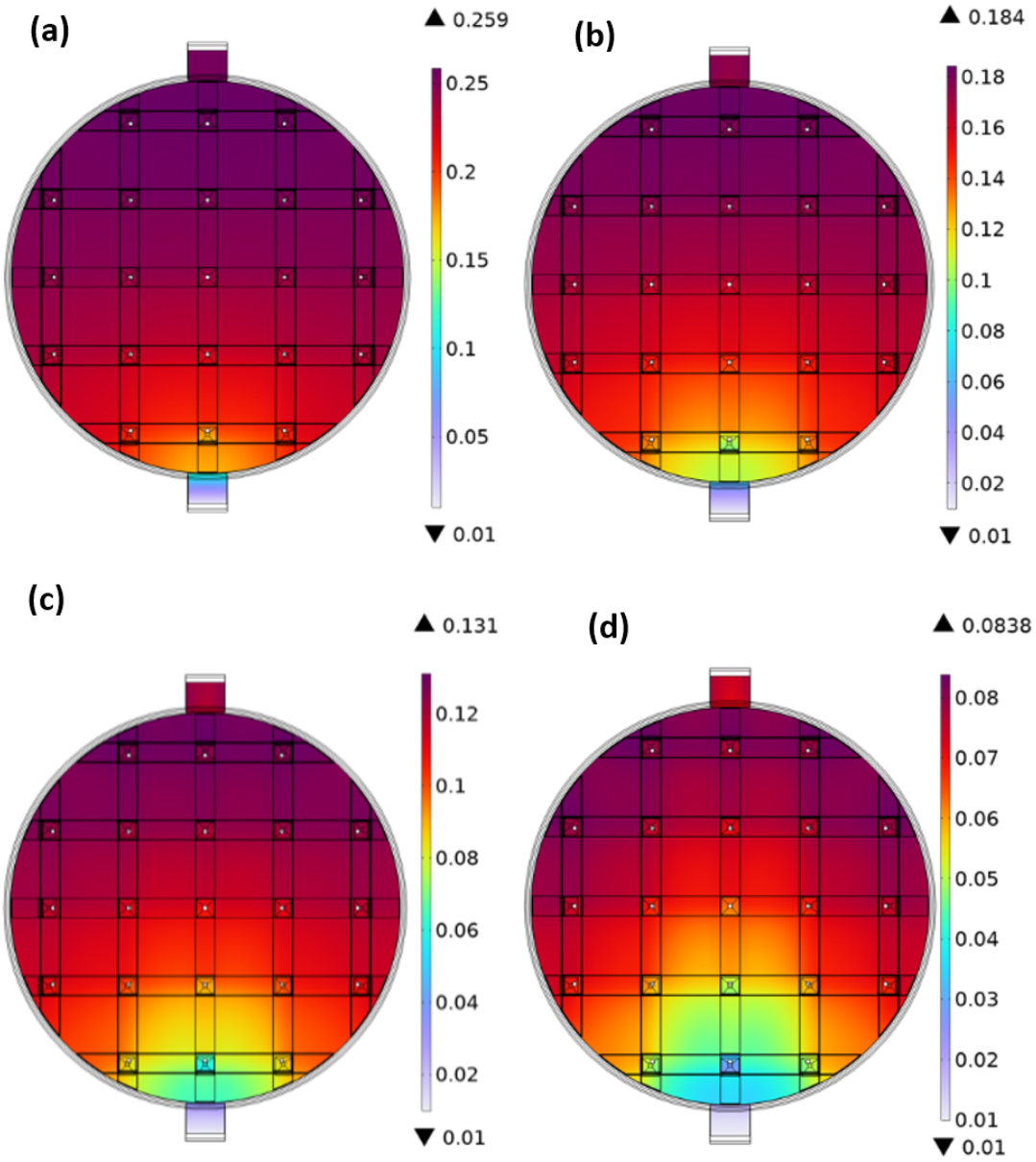

Figure 5. Gas volume fraction distribution in flow channels for 24 pyramidal pins, (a) $v_{in} = 0.01\ m/s$, (b) $v_{in} = 0.05\ m/s$, (c) (a) $v_{in} = 0.1\ m/s$, and (a) $v_{in} = 0.2\ m/s$.

development of efficient designs of next-generation alkaline electrolyzers.

ACKNOWLEDGEMENTS

This project has received funding from the European Union HORIZON Research and Innovation Actions under grant agreement ID 101122323 (UKRI reference No 10106958, and ERC/ HORIZON-HLTH-2021-IND-07, grant No 101057430).

Funded by the European Union. Views and opinions expressed are however those of the author(s) only and do not necessarily reflect those of the European Union. Neither the European Union nor the granting authority can be held responsible for them.

AUTHOR IDENTIFIERS

Author ORCIDs:
Venkateshwarlu, Akepogu: 0000-0002-6874-9531
Li Puma, Gianluca: 0000-0002-9168-6284

DISCLAIMER

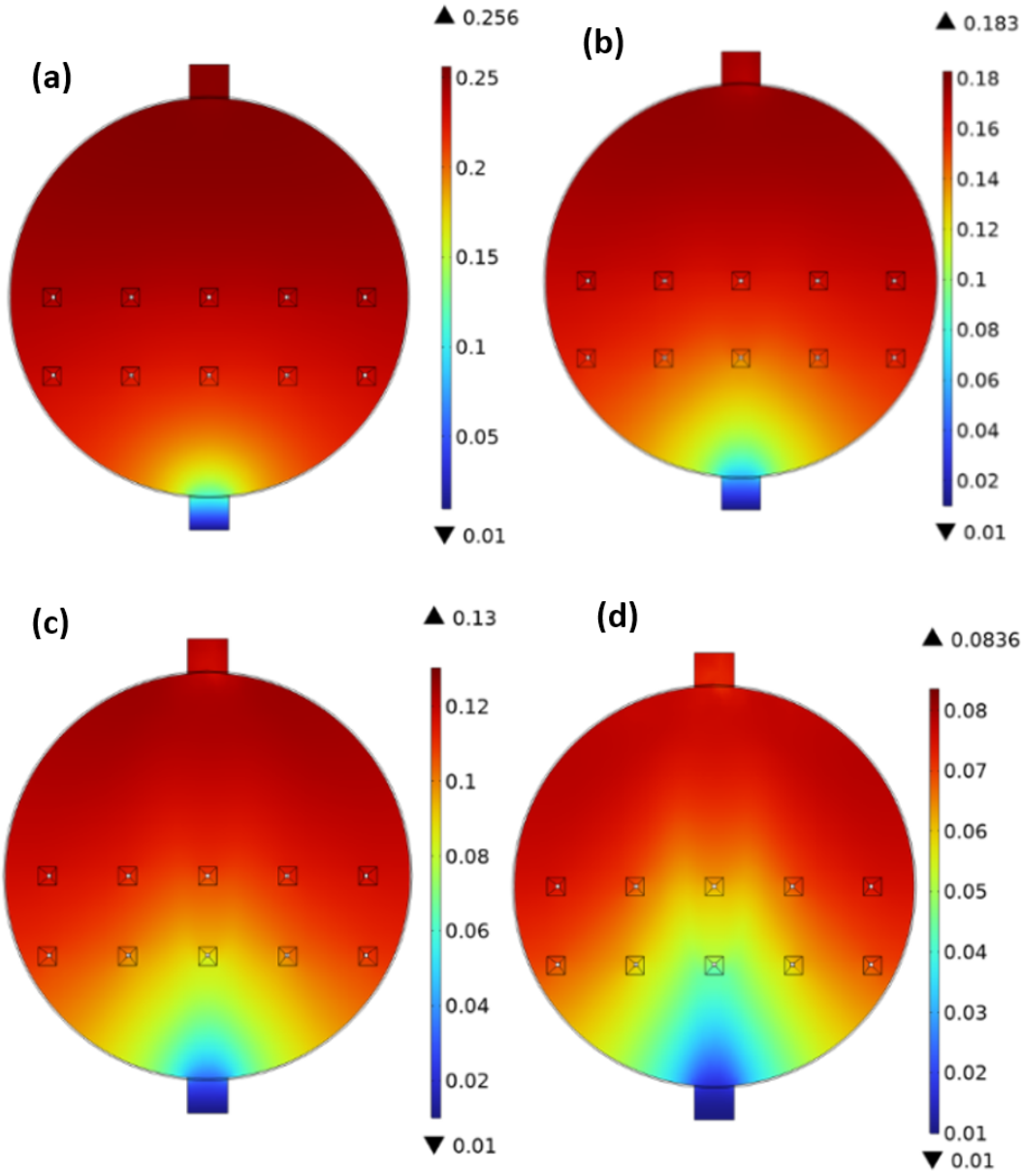

Figure 6. Gas volume fraction distribution in flow channels for 10 pyramidal pins, (a) $v_{in} = 0.01\ m/s$, (b) $v_{in} = 0.05\ m/s$, (c) (a) $v_{in} = 0.1\ m/s$, and (a) $v_{in} = 0.2\ m/s$.

Benyahia, Brahim: 0000-0002-5397-1498

REFERENCES

1. Shin H, Jang D, Lee S, Cho HS, Kim KH, Kang S. Techno-economic evaluation of green hydrogen production with low-temperature water electrolysis technologies directly coupled with renewable power sources. Energy Conversion and Management 286:117083 (2023). https://doi.org/10.1016/j.enconman.2023.117083
2. Riaz MA, Trogadas P, Aymé-Perrot D, Sachs C, Dubouis N, Girault H, Coppens MO. Water electrolysis technologies: the importance of new cell designs and fundamental modelling to guide industrial-scale development. Energy Environ. Sci. 18:5190-5214 (2025). https://doi.org/10.1039/d4ee05559d
3. Risco-Bravo A, Varela C, Bartels J, Zondervan E. From green hydrogen to electricity: a review on recent advances, challenges, and opportunities on power-to-hydrogen-to-power systems. Renewable and Sustainable Energy Reviews 189:113930 (2024). https://doi.org/10.1016/j.rser.2023.113930

4. Zhang W, Liu M, Gu X, Shi Y, Deng Z, Cai N. Water electrolysis toward elevated temperature: advances, challenges and frontiers. Chem. Rev. 123:7119-7192 (2023). https://doi.org/10.1021/acs.chemrev.2c00573
5. Luo S, Zhang T, Xu H, Zhang J, Zhao H, Yun J, Zhao H. Optimizing alkaline water electrolysis: a dual-model approach for enhanced hydrogen production efficiency. Energies 17:5512 (2024). https://doi.org/10.3390/en17215512
6. Zarghami A, Deen NG, Vreman AW. CFD modeling of multiphase flow in an alkaline water electrolyzer. Chemical Engineering Science 227:115926 (2020). https://doi.org/10.1016/j.ces.2020.115926
7. Jang D, Cho HS, Kang S. Numerical modeling and analysis of the effect of pressure on the performance of an alkaline water electrolysis system. Applied Energy 287:116554 (2021). https://doi.org/10.1016/j.apenergy.2021.116554
8. Hu S, Guo B, Ding S, Yang F, Dang J, Liu B, Gu J, Ma J, Ouyang M. A comprehensive review of alkaline water electrolysis mathematical modeling. Applied Energy 327:120099 (2022). https://doi.org/10.1016/j.apenergy.2022.120099
9. Gu H, Wu Q, Zhang M, Xu X, Yu J, Bai Y, Wang Y. Enhancing gas-liquid distribution uniformity in alkaline water electrolyzers by an innovative inlet array structure, a numerical study. Renewable Energy 256:124407 (2026). https://doi.org/10.1016/j.renene.2025.124407
10. Gong Y, Shen N, Zhang B, Xing P, Liu Q, Yu Z, Tan J, Ma X. Gas-liquid flow and electrochemical reactions involved in AEM water electrolytic cells: numerical simulation and parameter analysis. Fuel 409:137925 (2026). https://doi.org/10.1016/j.fuel.2025.137925
11. Hu R, Wen C, Ye Z, Qi Y, Zhang B, Kang K, Gao Y, Wang D, Tu Z. A comprehensive review of flow channel designs and optimizations for water electrolysis technology. Applied Energy 400:126643 (2025). https://doi.org/10.1016/j.apenergy.2025.126643
12. Liang H, Lin S, Zhao K, Liu P, Hu N, Song H, Yang Y, Zheng C, Zhang X, Gao X. Three-dimensional simulation of alkaline electrolyzer with an advanced partitioned point flow channel. International Journal of Hydrogen Energy 86:1252-1261 (2024). https://doi.org/10.1016/j.ijhydene.2024.09.015
13. Wei X, Umehara Y, Nakajima H, Ito K, Etoh A, Mori S. Effect of mesh size of ni wire mesh electrodes on alkaline water electrolysis performance: a study based on the observation of bubble departure behavior. International Journal of Hydrogen Energy 120:189-200 (2025). https://doi.org/10.1016/j.ijhydene.2025.03.267
14. Kimuli EN, Onyemelukwe II, Benyahia B, Rielly CD. Characterisation of axial dispersion in a meso-scale oscillatory baffled crystalliser using a numerical approach. In: Espuña A, Graells M, Puigjaner L, editors. *Computer Aided Chemical Engineering*. Elsevier. 40:223–228 (2017). https://doi.org/10.1016/B978-0-444-63965-3.50039-8
15. Benyahia B, Bandulasena MV, Bandulasena HCH, Vladisavljevi? GT. Experimental and computational analysis of mixing inside droplets for microfluidic fabrication of gold nanoparticles. Ind. Eng. Chem. Res. 60:13967-13978 (2021). https://doi.org/10.1021/acs.iecr.1c01960
16. Courtais A, Lesage F, Privat Y, Pelaingre C, Latifi AM. Cfd-based geometrical shape optimization of a packed-bed reactor combining multi-objective and adjoint system methods. Chemical Engineering Science 275:118728 (2023). https://doi.org/10.1016/j.ces.2023.118728
17. Schalenbach M, Tjarks G, Carmo M, Lueke W, Mueller M, Stolten D. Acidic or alkaline? towards a new perspective on the efficiency of water electrolysis. J. Electrochem. Soc. 163:F3197-F3208 (2016). https://doi.org/10.1149/2.0271611jes